Accepted Manuscript

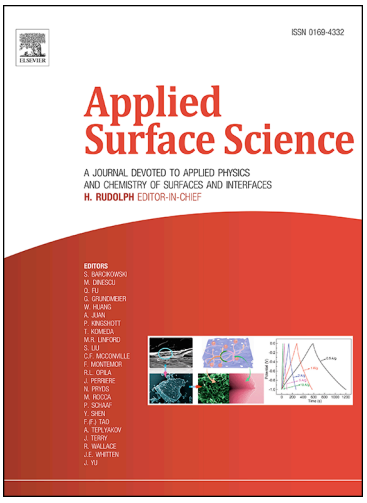

Full Length Article

Effect of grain boundaries on the interfacial behaviour of graphene-polyethylene nanocomposite

Akarsh Verma, Avinash Parashar, M. Packirisamy

PII: S0169-4332(18)33297-5
DOI: https://doi.org/10.1016/j.apsusc.2018.11.218
Reference: APSUSC 41064

To appear in: *Applied Surface Science*

Received Date: 24 October 2018
Revised Date: 24 November 2018
Accepted Date: 27 November 2018

Please cite this article as: A. Verma, A. Parashar, M. Packirisamy, Effect of grain boundaries on the interfacial behaviour of graphene-polyethylene nanocomposite, *Applied Surface Science* (2018), doi: https://doi.org/10.1016/j.apsusc.2018.11.218

Effect of grain boundaries on the interfacial behaviour of graphene-polyethylene nanocomposite

Akarsh Verma[a], **Avinash Parashar**[a]* and **M. Packirisamy**[b]

[a] Department of Mechanical and Industrial Engineering, Indian Institute of Technology, Roorkee, India
[b] Department of Mechanical, Industrial and Aerospace Engineering, Concordia University, Montreal, Canada

Abstract:

Aim of this article was to investigate the effect of grain boundaries on the interfacial properties of bi-crystalline graphene/polyethylene based nanocomposites. Molecular dynamics based atomistic simulations were performed in conjunction with the reactive force field parameters to capture atomic interactions within graphene and polyethylene atoms, whereas non-bonded interactions were considered for the interfacial properties. Atoms at the higher energy state in bi-crystalline graphene helps in improving the interaction at the nanocomposite interphase. Geometrical imperfections such as wrinkles and ripples helps the bi-crystalline graphene in increasing the number of adhesion points between the nanofiller and matrix, which eventually improves the strength and toughness of nanocomposite. These outcomes will help in opening new opportunities for defective nanofillers in the development of nanocomposites for future applications.

Keywords: Graphene, Grain boundaries, Polyethylene, Molecular dynamics, Reactive force field, Nanocomposites

*Corresponding author. E-mail: drap1fme@iitr.ac.in; Ph: +91-1332284801 (Avinash Parashar)

1. Introduction

Graphene is a two-dimensional (2D) nanomaterial with honeycomb crystal lattice domain [1, 2]. Due to exceptional mechanical, thermal and electrical properties, graphene is emerging as a potential candidate for the reinforcement of nanocomposites [3-5]. In addition to structural applications, graphene has wide range of application in the field of electronics [6], biotechnology [7], desalination membrane [8], clean energy devices [9], photocatalyst [10] and hydrogen storage [11].

In thermoplastic based nanocomposites, polyethylene (PE) is a leading matrix material with low cost and average mechanical properties. Due to easy processability and insulating behaviour, PE based composites are used for the manufacturing of armour materials, pipes, packaging and also as biomaterial [12, 13]. Higher content of hydrogen (the element with lowest atomic mass) in PE also helps in extending its application to space structures and for radiation shielding [14, 15]. Molecular chain structure of PE contains both amorphous as well as crystalline structure, which governs the increment in mechanical stiffness and flexibility [13, 15]. These atomistic scale phenomena cannot be easily captured by conventional experimental techniques. Atomistic modelling techniques such as molecular dynamics (MD) have proved to be viable in simulating the nanoscale dynamics of intricate PE structure [16, 17].

Several computational studies on graphene/PE nanocomposites have already been reported in the literature [18-26]. Jin et al. [24] revealed enhancement in interfacial mechanical properties of functionalised graphene and PE based nanocomposite. They attributed higher interfacial strength for relatively stronger covalent bonds formed by the functional groups as compared to weak non-bonded van der Waals interactions. Li et al. [27, 28] reported that the Stone-Thrower-Wales (STW) defects also helps in enhancing the interfacial shear strength

and thermal conductivity between defected graphene and epoxy. Ma et al. [29] chemically functionalised the graphene with 4,4-diaminophenylsulfone and studied the mechanical and fracture behaviour of epoxy based nanocomposite. Their simulations predicted that the functionalised interface helps in improving young's modulus and fracture release rate by 47.7% and 84.6%, respectively. Lv et al. [30] also captured the effect of chemical functionalisation of interface between graphene/PE nanocomposite. They reported an overall enhancement in the bonding energy and shear stress for the nanocomposite system. Ding et al. [31] predicted a superior interfacial strength for graphene oxide based nanocomposites, as compared to pristine form of graphene. Ramanathan et al. [32] experimentally described the positive impact of functionalised graphene sheets on the mechanical and thermal behaviour of poly(methyl methacrylate) composite. Liu et al. [33] concluded in their work that grafting of graphene with polymer chains helps in improving the shear strength as well as graphene's dispersion in the polymer matrix. Recently in 2018, Rajesh and Avinash [12] performed atomistic simulations to study the effect of defective h-BN nanosheets on the PE based nanocomposites. An overall improvement in the interfacial strength as well as mechanical properties of h-BN/PE nanocomposite was predicted in their computational work. Due to limitations associated with the synthesising techniques, nanomaterials e.g. large size graphene nanosheets are synthesised with geometrical defects such as vacancies, dislocations and grain boundaries (GB) [34, 35]. Scanning tunneling microscopy and transmission electron microscopy based experimental characterization of polycrystalline graphene reveals that GB configuration is composed of pentagon-heptagon (5–7) rings [36, 37]. Several computational and experimental works have already been performed to characterize the mechanical properties of bi-crystalline graphene [38-42]. Xu et al. [38] predicted decline in the mechanical properties of bi-crystalline graphene as compared to pristine counterpart. Yang et al. [39] and Grantab et al. [40] employed the MD based atomistic simulations to

predict the brittle behavior of bi-crystalline graphene configurations. Recently, our research with oxidized bi-crystalline graphene nanosheets have predicted a shift in the failure morphology from brittle to ductile with specific spatial distribution of oxide groups [41, 42].

So far, research was mostly focused on using either pristine or chemically functionalised graphene for the reinforcement of polymer based nanocomposites. But, larger size nanosheets are considered as a better reinforcement for the nanocomposites. Chemical vapour deposition is the most commonly used technique for synthesising larger size graphene, but it results in polycrystalline structure. Literature is almost mute on the effect of grain boundaries on the reinforcing capabilities of graphene for polymer based nanocomposites. So taking this as our motivation and in order to fulfil this literature gap, herein this article, the authors have attempted to elucidate the role of GB in graphene domain on the interfacial bonding characteristics.

2. Modelling details

In this study, the classical mechanics based MD approach was used to perform all the simulations. In order to capture the interatomic interactions between carbon in graphene and carbon and hydrogen atoms in PE, reactive force field (ReaxFF) parameters proposed by Chenoweth et al. [43] has been used; whereas, for the cross or interfacial (van der Waals) interactions between graphene and PE, Lennard-Jones (LJ) potential parameters (refer Table 1) were employed from the literature work [44-46].

Table 1. LJ potential parameters for carbon (C) and hydrogen (H) atoms.

Atom species	Energy constant, ϵ (eV)	Distance constant, σ (Å)
H	0.000867	2.995
C (in PE)	0.002342	4.010
C (in graphene)	0.002390	3.412

ReaxFF is comparatively complex and computationally intensive, but possess quantum-chemical accuracy to capture the bond dynamics and charge transference in C/H/O atoms [47]. Mathematically, ReaxFF provides the total potential energy of molecular system (E_{system}) in accordance with equation 1:

$$\mathbf{E_{system} = E_{bond} + E_{over} + E_{angle} + E_{tors} + E_{vdWaals} + E_{coulomb} + E_{specific}} \quad \mathbf{(1)}$$

where, $\mathbf{E_{bond}}$ describes the energy contribution due to bond formation between atoms; $\mathbf{E_{over}}$ is an energy penalty that prevents the over coordination of atoms; $\mathbf{E_{angle}}$ and $\mathbf{E_{tors}}$ report the energies associated with three-body valence angle strain and four-body torsional angles; $\mathbf{E_{vdWaals}}$ and $\mathbf{E_{coulomb}}$ are the van der Waals and Coulomb interaction energies; $\mathbf{E_{specific}}$ is for system specific terms that encompasses lone-pair, hydrogen-binding and conjugate bonds corrections [48]. The neighbour cut-off and hydrogen bonding distance parameters were fixed at 4.5 and 6 Å, respectively [49].

All the MD simulations were performed in open source code software, large-scale atomic/molecular massively parallel simulator (LAMMPS) [50-52], whereas post processing of the dump files were performed with the help of open visualization tool (OVITO) [53]. Periodic boundary conditions were imposed in all the principal directions to minimize the finite size/free edges effect. Schematic of the atomistic system of nanocomposite containing

PE along with pristine and bi-crystalline graphene is shown in Fig.1. In this article, six different set of GB configurations along zigzag (ZZ) and armchair (AC) directions were generated. GB energies for each atomic configuration with respect to mis-orientation angle were earlier estimated in our previous articles [41, 42]. Henceforth, eight different configurations were considered that includes, (a) neat PE (referred as Neat PE), (b) PE reinforced with pristine graphene (referred as PE/GRP), (c) PE reinforced with graphene containing GB in the ZZ direction with a mis-orientation angle of 21.8° (referred as PE/ZZ 21.8), (d) PE reinforced with graphene containing GB in the ZZ direction with a mis-orientation angle of 13.2° (referred as PE/ZZ 13.2), (e) PE reinforced with graphene containing GB in the ZZ direction with a mis-orientation angle of 9.43° (referred as PE/ZZ 9.43), (f) PE reinforced with graphene containing GB in the AC direction with a mis-orientation angle of 27.8° (referred as PE/AC 27.8), (g) PE reinforced with graphene containing GB in the AC direction with a mis-orientation angle of 21.8° (referred as PE/AC 21.8), and (h) PE reinforced with graphene containing GB in the AC direction with a mis-orientation angle of 17.9° (referred as PE/AC 17.9). In all these aforementioned configurations, the bi-crystals of graphene nanosheets were randomly oriented in the PE matrix for maintaining the realistic condition. Also, the weight percentage of both pristine and bi-crystalline graphene sheets as a reinforcement in the nanocomposite were kept in the range of 2.9-3.1%.

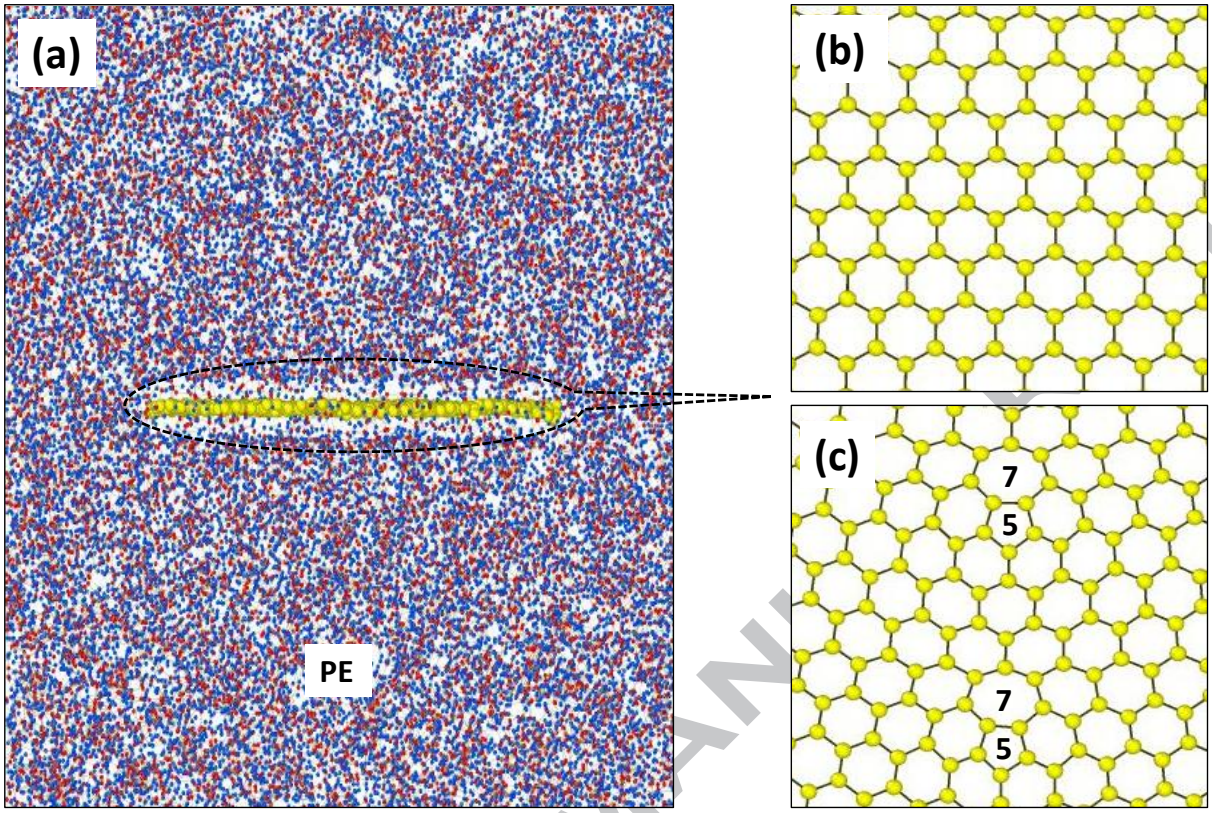

Fig.1. (a) PE/GRP nanocomposite system, (b) pristine graphene nanosheet, and (c) ZZ 13.2 graphene nanosheet (Red, blue and yellow colored spheres designate PE carbon atoms, PE hydrogen atoms and graphene carbon atoms, respectively) (7-5 indicates the heptagon and pentagon that is formed at the GB)

All the simulations were performed at a temperature of 100 K (below glass transition temperature of PE), and tensile deformation in uni-axial direction was applied at a strain rate of 10^{-3} ps^{-1}. During the tensile deformation in uni-axial direction, zero pressure was maintained in direction transverse to loading. A cubical supercell size of 70 Å × 70 Å × 70 Å was used to pack PE molecular chains, which helps in maintaining a high density of approximately 0.88-0.91 g/cm^3. After assigning the atomic coordinates of graphene and PE chains, energy of the system was minimised with the help of conjugate gradient algorithm. Subsequently, system equilibration was performed with the help of canonical NVT (constant

number of atoms, volume and temperature) ensemble at 500 K for 10^6 time steps with Langevin thermostat controlling the temperature. In the next phase, system temperature was slowly cooled down to 100 K through isothermal-isobaric (NPT) ensemble for 25 ps. Finally, the system was relaxed again under the influence of NPT ensemble at 100 K for a total time period of 25 ps. During the entire equilibration process, integration time step was kept constant at 0.15 fs. In all the simulations, the charge equilibration was also performed after every ten integration steps.

In order to predict the per-atom stress components and for stress tensor calculations, the virial stresses [54-56] were calculated with the help of equation 2:

$$\boldsymbol{\sigma_{ij}^{\alpha} = \frac{1}{\varphi^{\alpha}}\left(\frac{1}{2}\mathbf{m^{\alpha}v_i^{\alpha}v_j^{\alpha}} + \sum_{\beta=1,n}\mathbf{r_{\alpha\beta}^{j}f_{\alpha\beta}^{i}}\right)} \qquad \textbf{(2)}$$

where, $r_{\alpha\beta}$ is distance between the atoms α and β; m^{α} and v^{α} are the mass and velocity of atom α; φ^{α} is the atomic volume of system; i and j stand for indices in Cartesian coordinate system; α and β being the atomic indices. For avoiding the stress fluctuations during tensile strain analysis, Velocity-Verlet algorithm with a relatively smaller integration time step of 0.15 fs was opted.

3. Results and discussions

3.1. Effect of defected graphene on the tensile strength of PE nanocomposites

ReaxFF potential parameters have already been validated for simulating the mechanical properties of pristine and bi-crystalline graphene in our previous articles [41, 57]. In order to validate the accuracy of ReaxFF for capturing the tensile deformation in PE, simulations were performed with neat PE subjected to uni-axial tension; the stress-strain response obtained is plotted in Fig.2. This stress-strain behavior was found to be in good agreement with the

results reported in literature [14, 58, 59]. In this computational work, the maximum stress before the softening was refereed as tensile strength. After validating the ReaxFF parameters for neat PE, next set of simulations were performed after reinforcing PE with pristine form of graphene. Stress-strain response obtained from the uni-axial tensile deformation of PE/GRP is plotted in Fig.2, and an overall improvement in tensile strength of 85.4% was predicted for the nanocomposite as compared to neat PE.

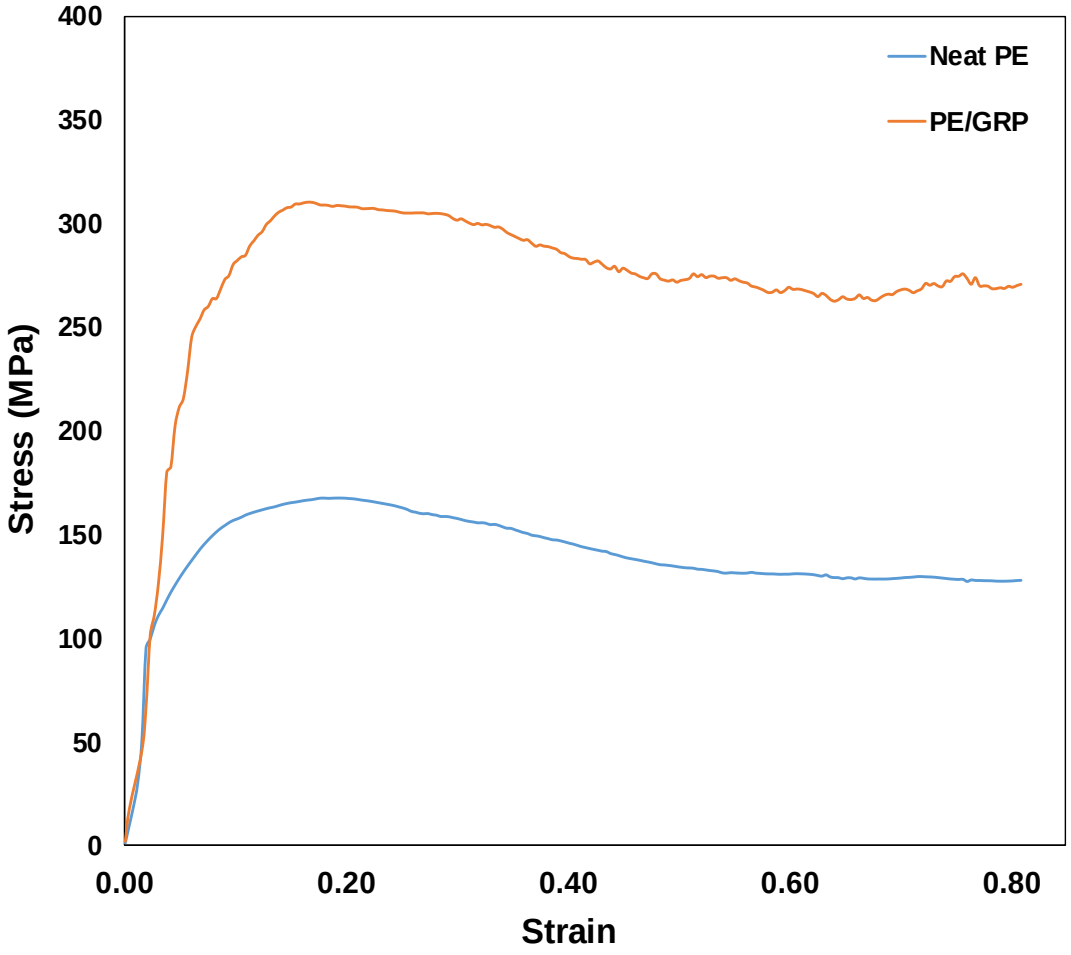

Fig.2. Stress-strain response of neat polyethylene and PE/GRP system subjected to uniaxial tensile load

In addition to tensile strength, significant improvement in the toughness of nanocomposite was also observed in nanocomposite as compared to neat PE, which motivates the researchers

to develop PE based nanocomposites for future armour materials. Properties of nanocomposites are governed by the interface between the matrix and nanofiller. Thus, for the same percentage of reinforcement in nanocomposite, a higher degree of interfacial strength is desirable; which can be achieved by either functionalising the interface or inducing geometrical defects in the nanofillers domain. Surface-functionalisation of the reinforcement with radical groups tend to convert the weak non-bonded (van der Waals) interaction to relatively stronger chemical bonded interactions; thereby increasing the interaction energy. While on the other hand, as material defects are the high energy sites, there creation on reinforcement surface would induce structural changes that may augment the non-bonded interactions. However, chemical functionalisation and geometrical defects deteriorate the properties of nanofiller itself.

In the next phase of simulations, graphene nanosheets containing different type of GB configurations were used for reinforcing PE based nanocomposites. Stress-strain responses for different types of bi-crystalline graphene reinforced PE nanocomposites are plotted in Fig.3 and Fig.4 for AC and ZZ configurations of graphene, respectively. It can be inferred from Fig.3 and Fig.4 that as compared to pristine graphene, bi-crystalline graphene is a superior nanofiller for reinforcing PE matrix.

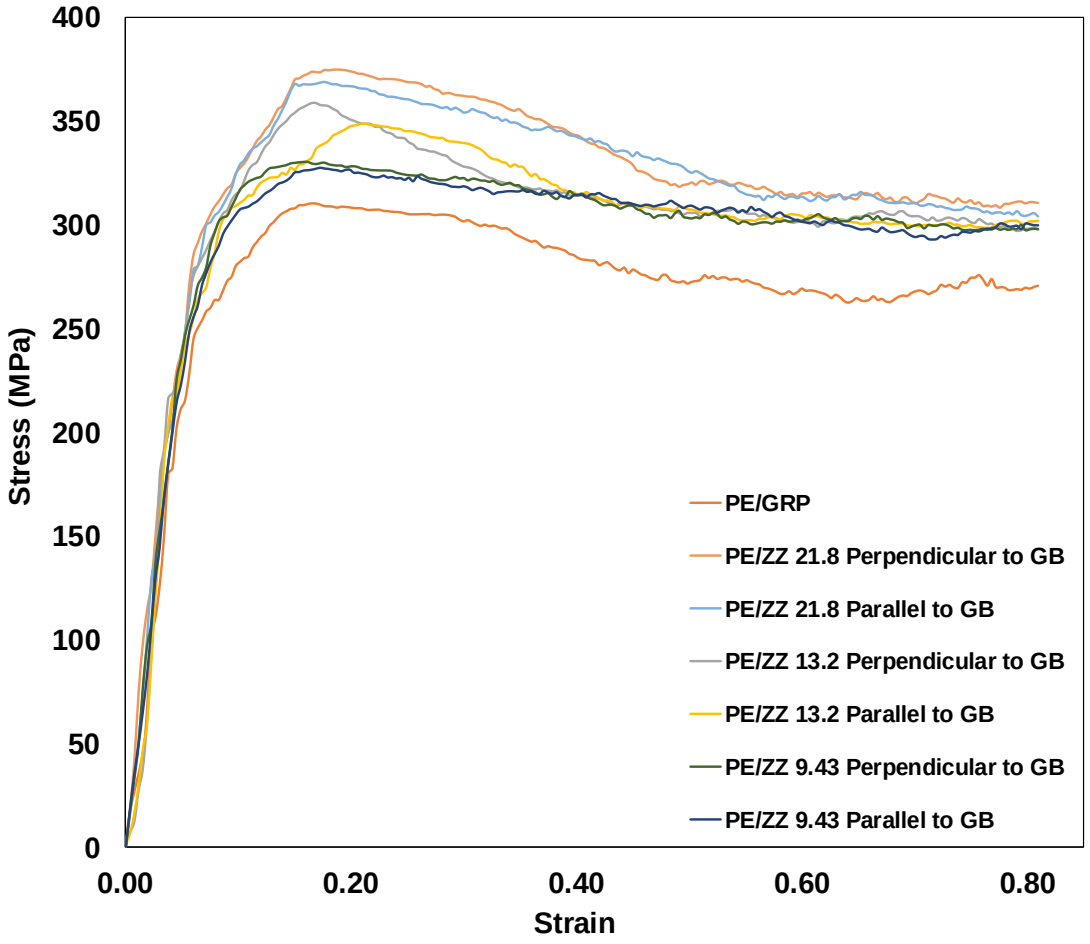

Fig.3. Stress-strain response of PE/GRP and PE/ZZ system subjected to uniaxial tensile load (Perpendicular to GB means tensile load is in the direction perpendicular to GB and same with parallel to GB)

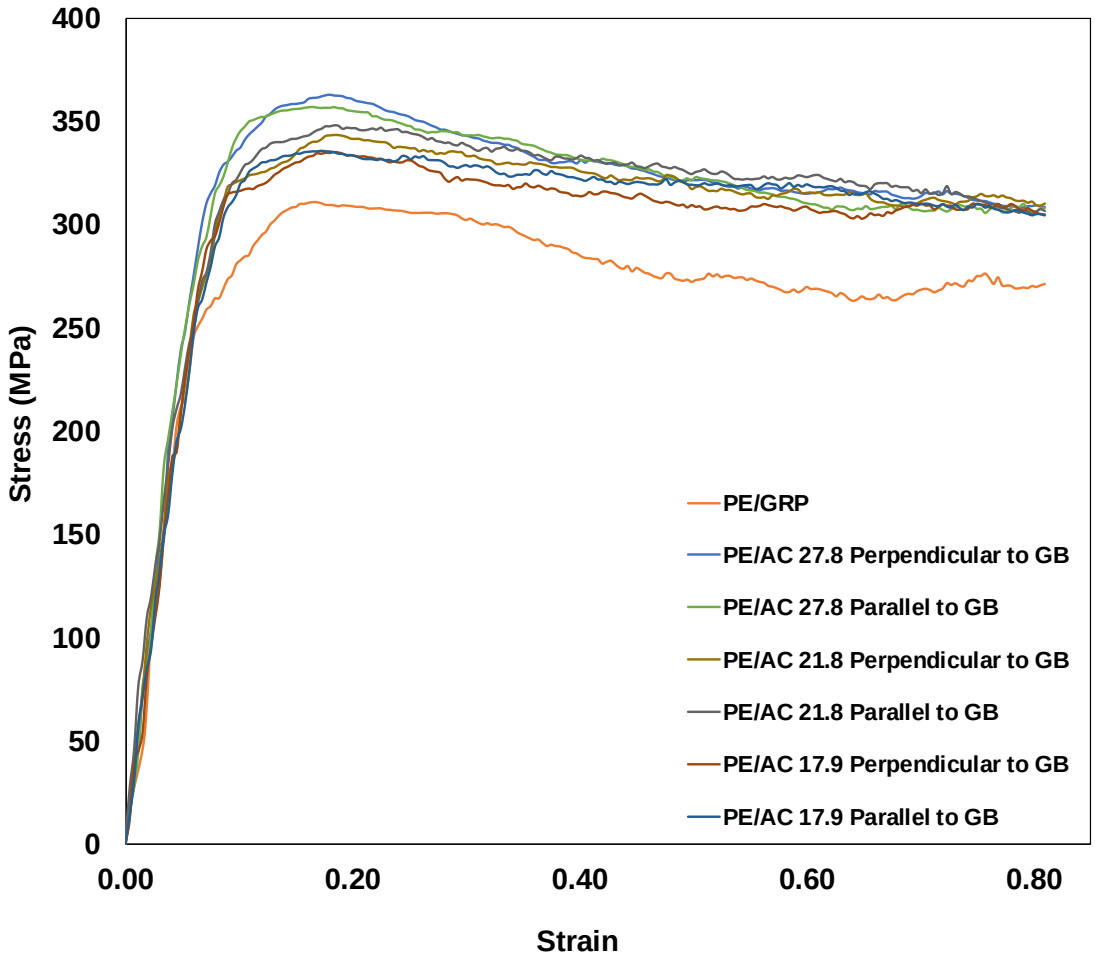

Fig.4. Stress-strain response of PE/GRP and PE/AC system subjected to uniaxial tensile load (Perpendicular to GB means tensile load is in the direction perpendicular to GB and same with parallel to GB)

Superior reinforcement capabilities displayed by bi-crystalline graphene is attributed to more number of atoms in the higher energy state, which helps in achieving better non-bonded interactions with the PE chains. Due to increased interaction, atoms configuring GB atoms were actually pulled by the PE chains that results in inducing wrinkles (crests and troughs) in the 2D bi-crystalline graphene; in contrast, the pristine graphene structure in PE/GRP nanocomposite relatively remained flattened (minimal out of plane displacement) during tensile deformation as captured in Fig.5. Curved configuration helps in increasing the contact

points between bi-crystalline graphene and PE chains, which eventually improves the non-bonded interaction between nanofiller and matrix. In addition to chemical interactions, mechanical bonding between the bi-crystalline graphene and PE chains has also been improved in curved configuration of nanofillers. It can also be inferred from the stress-strain responses plotted in Fig.3 and Fig.4 that increment in tensile strength of nanocomposites is more prominent in bi-crystalline graphene containing higher mis-orientation angles. Density of atoms contained by the GB in lower mis-orientation angle is lower as compared to higher angle. Higher mis-orientation angle configurations lead to redistribution of stress uniformly throughout the bi-crystalline graphene sheet that maximizes the load transfer phenomenon and helps in improving the tensile strength. It is predicted from the post processing of dump files that higher mis-orientation angle configurations contain more energetic sites (due to high density of dislocations) relative to lower mis-orientation angles for a given weight percentage of graphene in PE; therefore, there would be more wrinkling in higher mis-orientation angles and thus high tensile strength. These explanations can also be found and related to our earlier research articles [41, 42] in conjunction with the recommendation of Grantab et al. [40] work; hence, it complements our current efforts. PE/ZZ 21.8 and PE/AC 27.8 are the superlative configurations, as they showcase the highest tensile strength amongst all other variations as tabulated in table 2. In each of the simulations, uniaxial tensile loading was applied perpendicular as well as parallel to the GB. Both these loading directions displayed approximately similar tensile strengths; thus, we predicted that tensile strength of GB defected PE/GRP system is independent to the loading direction. It was also predicted from the tensile deformation of above designed nanocomposites that after achieving the maximum tensile strength, permanent deformation in the form of voids and crazing starts generating in PE matrix as shown in Fig.6.

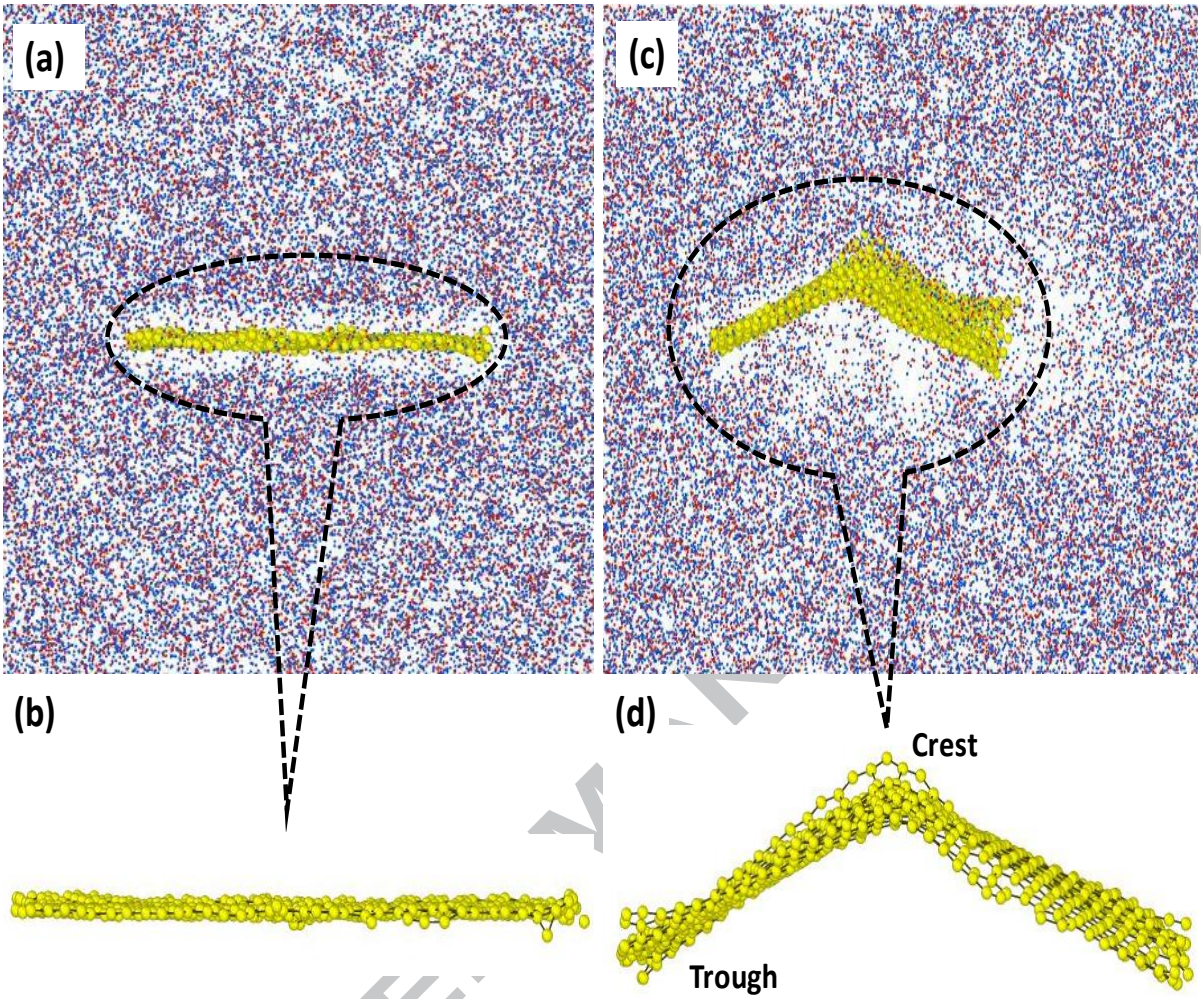

Fig.5. (a) PE/GRP nanocomposite system, (b) Isolated flat pristine graphene, (c) Snapshots revealing the formation of wrinkles in GB defected PE/GRP system subjected to tension, and (d) Isolated wrinkled bi-crystalline graphene

Table 2. Improvement in tensile strength for various configurations with respect to neat PE.

Configuration	*Tensile strength (MPa)*	*% Improvement*
Neat PE	167.52	-
PE/GRP	310.58	85.4
PE/ZZ 21.8	374.68	123.66
PE/ZZ 13.2	358.92	114.25
PE/ZZ 9.43	330.11	97.06
PE/AC 27.8	362.57	116.43
PE/AC 21.8	343.26	104.91
PE/AC 17.9	334.94	99.94

In order to further comprehend the physics behind the enhancement in tensile strength of nanocomposites reinforced with bi-crystalline graphene, authors have tabulated the values of interaction energy (ΔE) (with the help of equation 3) in table 3.

$$\mathbf{\Delta E = \left(E_{Total} - E_{PE} - E_{Graphene}\right)} \quad \textbf{(3)}$$

Where, E_{Total}, E_{PE} and $E_{Graphene}$ represent the total potential energies of whole composite system, polyethylene matrix and graphene (whether pristine or defected), respectively.

It can be observed from the data tabulated in table 3 that interaction energy is highest for nanocomposites reinforced with bi-crystalline graphene with higher mis-orientation angles. Additionally, better interfacial properties have been predicted from the interaction energy trend for bi-crystalline graphene nanocomposites as compared to pristine graphene.

Table 3. Interaction energies between nanofiller and PE matrix

Configuration	*Interaction energy (kcal/mol)*	*% Improvement*
PE/GRP	-1277	-
PE/ZZ 21.8	-1658	29.83
PE/ZZ 13.2	-1517	18.79
PE/ZZ 9.43	-1463	14.56
PE/AC 27.8	-1629	27.56
PE/AC 21.8	-1501	17.54
PE/AC 17.9	-1474	15.43

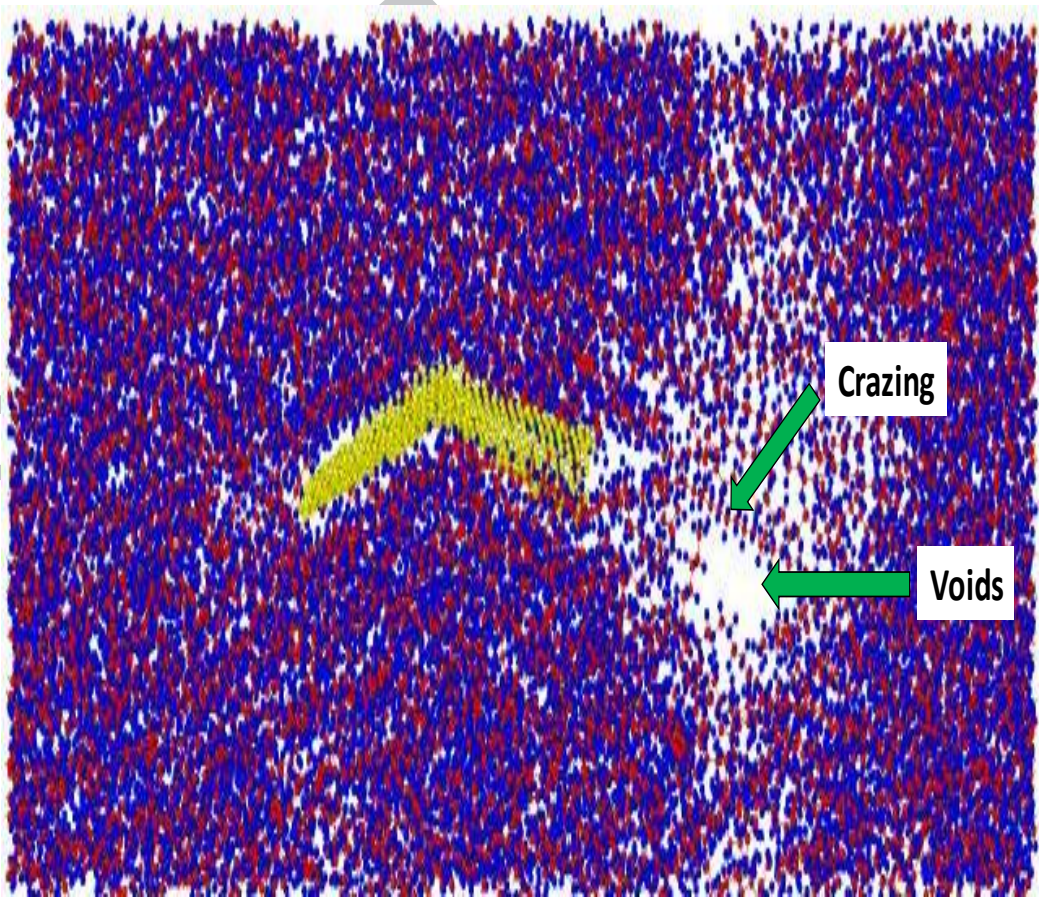

Fig.6. Snapshots showing crazing and voids formation in PE when subjected to tensile load

3.2. Effect of defected graphene on the shear strength of PE nanocomposites

After predicting tensile strength of nanocomposites, next set of simulations were performed to investigate the shear strength of the interface between graphene and PE matrix. In order to capture the shear strength at the interface, simulations were performed with periodic boundary conditions imposed only in two principal directions, whereas the third principal direction was used to pull the graphene out of polymer matrix as illustrated in Fig.7. In the graphene reinforced PE system, the pristine and bi-crystalline graphene nanosheets were pulled out of the PE matrix with a velocity of 0.0001 Å/fs along x-direction (non-periodic) and the resulting shear force on the graphene nanosheets in the pullout direction was plotted in Fig.8. During these set of simulations, graphene was considered as a rigid body, as the in-plane stiffness of 2D graphene is much higher than the PE matrix. The resulting maximum interfacial shear strength ($\tau_{xy\text{-}max}$) was calculated with the help of surface area of graphene nanosheet as per equation 4.

$$\boldsymbol{\tau_{xy-max} = \frac{F_{x-max}}{2A}} \quad \textbf{(4)}$$

Where, $F_{x\text{-}max}$ is the maximum force acting on graphene during the pull out process, and A is surface area of graphene nanosheet.

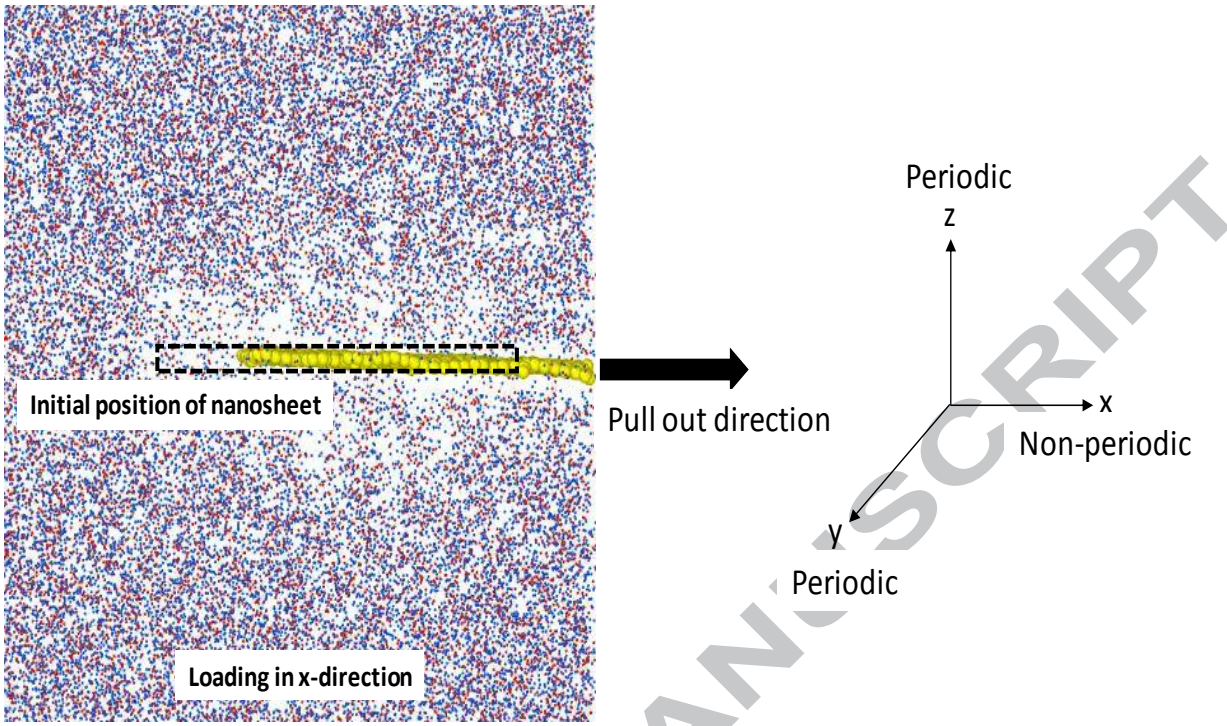

Fig.7. Atomistic model of the shear pull out simulation showing graphene being pulled out of the PE matrix

It can be inferred from Fig.8 that all the GB configurations in bi-crystalline graphene reinforcement have higher interfacial strength than the pristine PE/GRP nanocomposite. This enhanced behaviour is certainly due to the presence of high energy GB defect sites and their high adsorption capacity to the polymer molecules. Furthermore, GB increases the concentration of sp^2 carbon atoms near graphene surface, leading to improved π-π attractions at the PE and graphene interface. Thus, increase in the sliding resistance of PE on graphene sheet, eventually improves the interface properties. For the dependency of mis-orientation angle of GB, we found that the interfacial strength is directly proportional to the mis-orientation angle for both ZZ and AC directions. This is because the GB acts as an obstacle and there is no easy slipping of bi-crystalline graphene. More the mis-orientation angle, more is the GB dislocations density; thus, more is the obstacles and interfacial strength.

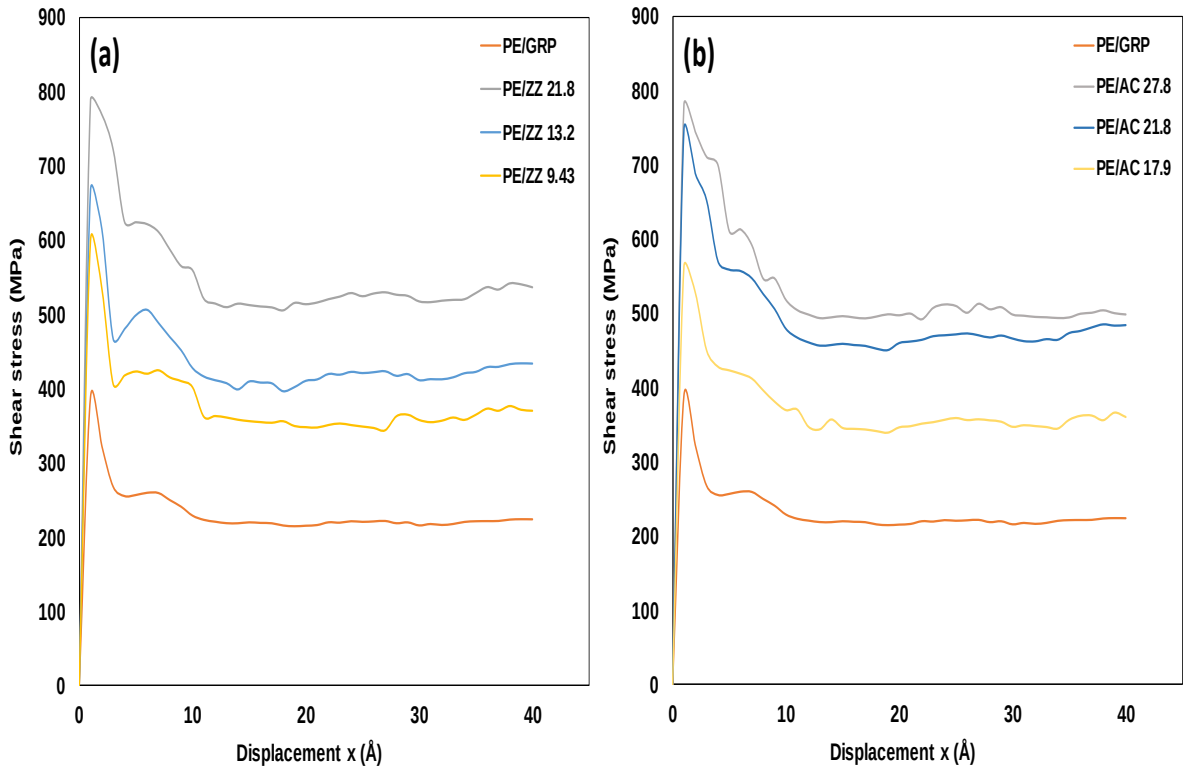

Fig.8. Interfacial shear strength ($\tau_{xy\text{-}max}$) vs displacement curves for various (a) ZZ, and (b) AC GB configurations of PE/GRP nanocomposite systems

3.3. Effect of defected graphene on the cohesive strength of PE nanocomposites

In the last subsection, simulations were performed to estimate the cohesive strength of interface for different configurations of nanocomposites. In order to estimate the cohesive strength, simulations were performed with tensile load applied in a direction perpendicular to the interface as illustrated in Fig.9. Once again non-periodic boundary conditions were imposed in the direction of loading as shown in Fig.9. In this part of research, the normal stress in direction of loading is plotted as a function of displacement in Fig.10.

The cohesive/normal strength (σ_{xx}) is calculated according to the equation 5.

$$\boldsymbol{\sigma_{xx}} = \frac{\boldsymbol{F_{xx-max}}}{\boldsymbol{A}} \quad \textbf{(5)}$$

Where, $F_{xx\text{-}max}$ is the maximum force acting on graphene nanosheet during the pull out process and A is the surface area of graphene nanosheet.

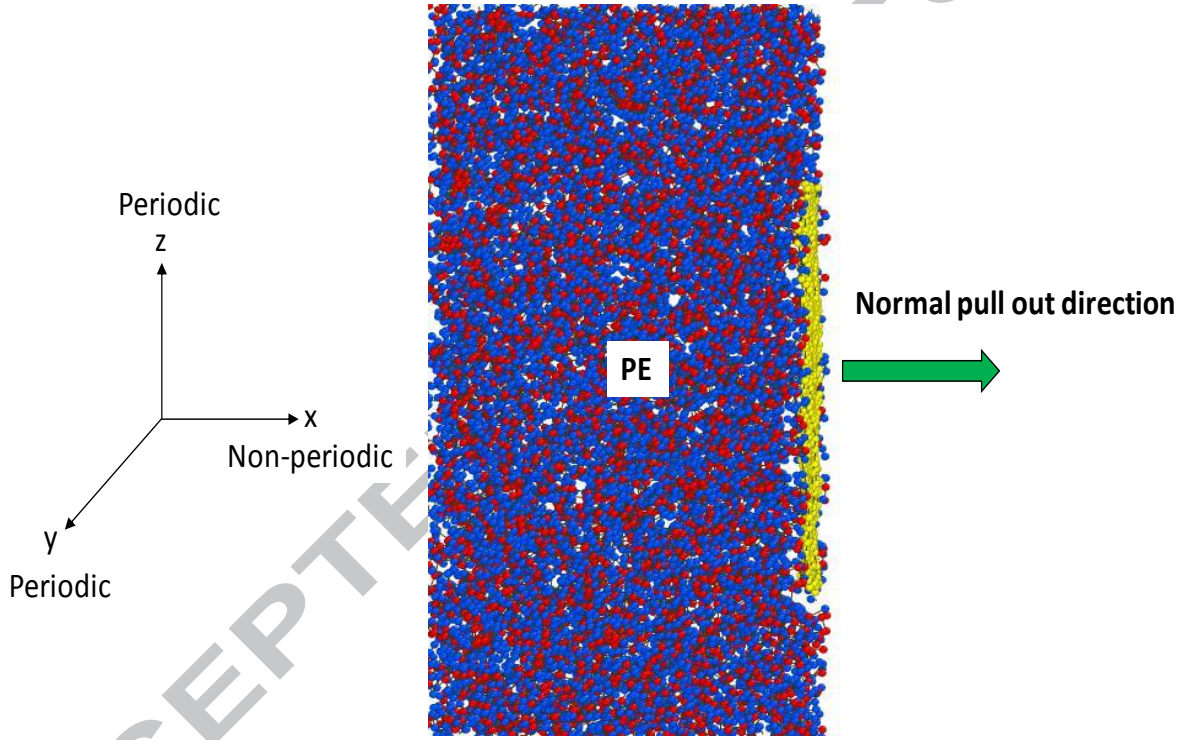

Fig.9. Atomistic model of the normal pull out simulation showing the graphene being pulled out of the PE matrix

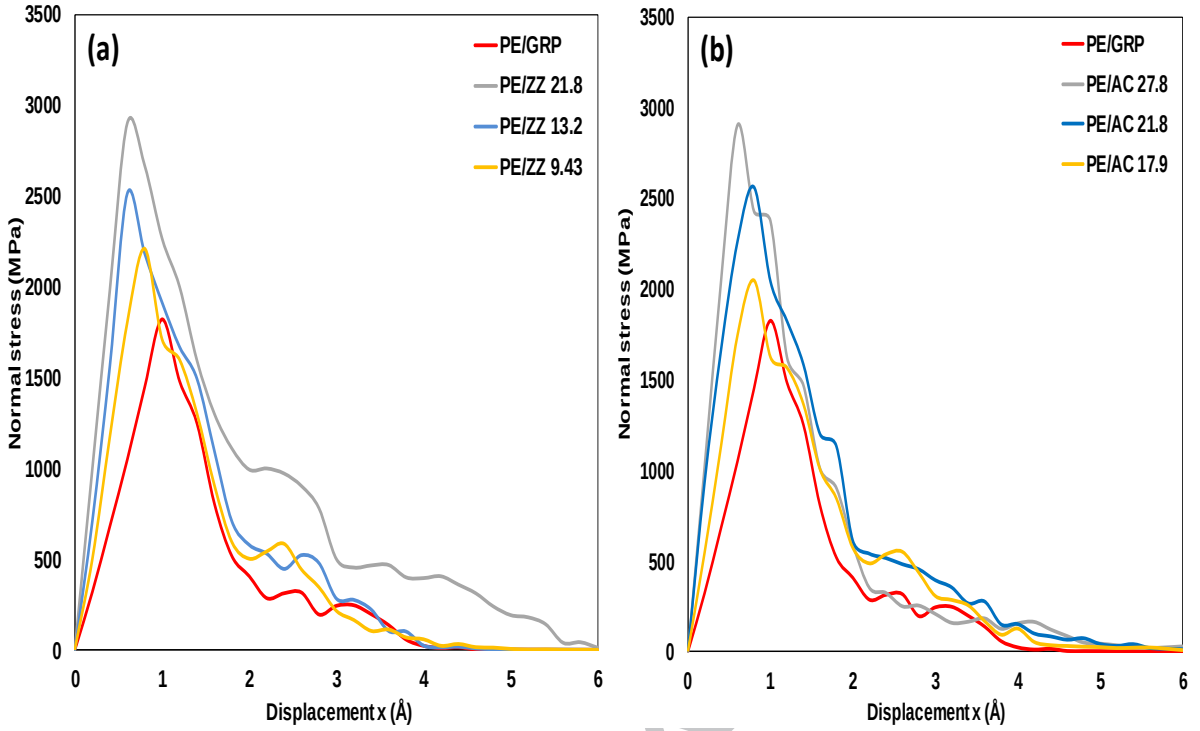

Fig.10. Normal stress (σ_{xx}) vs displacement curves for various (a) ZZ, and (b) AC GB configurations of PE/GRP nanocomposite systems

It can be inferred from the trend plotted in Fig.10 that similar to shear strength, normal interfacial stress of nanocomposite also improved significantly, while reinforced with bi-crystalline graphene as compared to pristine graphene. Hence, these GB act as the path for load transfer to take place and helps in establishing a strong mechanical interlocking with high cohesive strength. Higher mis-orientation angle GB configurations possess higher normal interfacial strength and vice-versa. As in higher mis-orientation angle GB, more GB dislocation space states become available for contact, which means that the interfacial strength values get enhanced. On a comparing note (Fig.8 and Fig.10), shear stress values at the interface are less than the cohesive/normal stress. This implies that the PE/GRP nanocomposites are more susceptible to fail via interfacial shear stress as compared to cohesive.

4.0 Conclusion

In summary, simulations were performed to study the reinforcing capabilities of bi-crystalline graphene as compared to pristine graphene nanosheet. All the simulations help in concluding that bi-crystalline graphene is a superior reinforcement for developing the future nanocomposites as compared to pristine PE nanocomposites. Significant improvement in the tensile, interfacial shear and normal cohesive strength of PE nanocomposite was reported with bi-crystalline graphene. We also perceived that wrinkling with substantial out-of-plane deformation in bi-crystalline graphene containing higher mis-orientation angle GB resulted in more number of adhesion points and better non-bonding interaction at the interface; which were the main mechanisms causing an increment in the tensile strength. These results will help in developing future nanocomposites with defective graphene as source of reinforcement. Despite the fact that polycrystalline graphene has lower strength as compared to pristine graphene, but emerges as a superior reinforcement for polymer based nanocomposites.

Conflicts of interest

"The authors declare no conflicts of interest."

Acknowledgements

Authors appreciatively acknowledge the financial support received from the Council of Scientific and Industrial Research (CSIR) and Department of Science and Technology (DST), India.

References

1. Novoselov, K.S., Fal, V.I., Colombo, L., Gellert, P.R., Schwab, M.G. and Kim, K., 2012. A roadmap for graphene. *Nature*, *490*(7419), p.192.

2. Geim, A.K., 2009. Graphene: status and prospects. *Science*, *324*(5934), pp.1530-1534.

3. Idowu, A., Boesl, B. and Agarwal, A., 2018. 3D graphene foam-reinforced polymer composites–A review. *Carbon*, *135*, pp.52-71.

4. Hsieh, S.H., Chen, W.J. and Yeh, T.H., 2015. Effect of various amounts of graphene oxide on the degradation characteristics of the ZnSe/graphene nanocomposites. *Applied Surface Science*, *358*, pp.63-69.

5. Verma, A., Parashar, A. and Packirisamy, M., 2018. Atomistic modeling of graphene/hexagonal boron nitride polymer nanocomposites: a review. *Wiley Interdisciplinary Reviews: Computational Molecular Science*, *8*(3), e1346.

6. Datta, D., Li, J., Koratkar, N. and Shenoy, V.B., 2014. Enhanced lithiation in defective graphene. *Carbon*, *80*, pp.305-310.

7. Wang, Y., Li, Z., Wang, J., Li, J. and Lin, Y., 2011. Graphene and graphene oxide: biofunctionalization and applications in biotechnology. *Trends in biotechnology*, *29*(5), pp.205-212.

8. Ang, E.Y., Ng, T.Y., Yeo, J., Liu, Z. and Geethalakshmi, K.R., 2016. Free-standing graphene slit membrane for enhanced desalination. *Carbon*, *110*, pp.350-355.

9. Zhu, Y., Murali, S., Cai, W., Li, X., Suk, J.W., Potts, J.R. and Ruoff, R.S., 2010. Graphene and graphene oxide: synthesis, properties, and applications. *Advanced materials*, *22*(35), pp.3906-3924.

10. Putri, L.K., Ong, W.J., Chang, W.S. and Chai, S.P., 2015. Heteroatom doped graphene in photocatalysis: a review. *Applied Surface Science*, *358*, pp.2-14.

11. Li, Y., Datta, D. and Li, Z., 2015. Anomalous mechanical characteristics of graphene with tilt grain boundaries tuned by hydrogenation. *Carbon*, *90*, pp.234-241.

12. Kumar, R. and Parashar, A., 2018. Effect of geometrical defects and functionalization on the interfacial strength of h-BN/polyethylene based nanocomposite. *Polymer*, *146*, pp.82-90.

13. Rahman, R. and Foster, J.T., 2014. Deformation mechanism of graphene in amorphous polyethylene: A molecular dynamics based study. *Computational Materials Science*, *87*, pp.232-240.

14. Hossain, D., Tschopp, M.A., Ward, D.K., Bouvard, J.L., Wang, P. and Horstemeyer, M.F., 2010. Molecular dynamics simulations of deformation mechanisms of amorphous polyethylene. *Polymer*, *51*(25), pp.6071-6083.

15. Chawla, R. and Sharma, S., 2017. Molecular dynamics simulation of carbon nanotube pull-out from polyethylene matrix. *Composites Science and Technology*, *144*, pp.169-177.

16. Yashiro, K., Naito, M., Ueno, S.I. and Jie, F., 2010. Molecular dynamics simulation of polyethylene under cyclic loading: Effect of loading condition and chain length. *International Journal of Mechanical Sciences*, *52*(2), pp.136-145.

17. Pant, P.K., Han, J., Smith, G.D. and Boyd, R.H., 1993. A molecular dynamics simulation of polyethylene. *The Journal of chemical physics*, *99*(1), pp.597-604.

18. Alian, A.R., Dewapriya, M.A.N. and Meguid, S.A., 2017. Molecular dynamics study of the reinforcement effect of graphene in multilayered polymer nanocomposites. *Materials & Design*, *124*, pp.47-57.

19. Yuan, Z., Lu, Z., Yang, Z., Sun, J. and Xie, F., 2016. A criterion for the normal properties of graphene/polymer interface. *Computational Materials Science*, *120*, pp.13-20.

20. Papageorgiou, D.G., Kinloch, I.A. and Young, R.J., 2017. Mechanical properties of graphene and graphene-based nanocomposites. *Progress in Materials Science*, *90*, pp.75-127.

21. Zhang, Y., Zhuang, X., Muthu, J., Mabrouki, T., Fontaine, M., Gong, Y. and Rabczuk, T., 2014. Load transfer of graphene/carbon nanotube/polyethylene hybrid nanocomposite by molecular dynamics simulation. *Composites Part B: Engineering*, *63*, pp.27-33.

22. Güryel, S., Walker, M., Geerlings, P., De Proft, F. and Wilson, M.R., 2017. Molecular dynamics simulations of the structure and the morphology of graphene/polymer nanocomposites. *Physical Chemistry Chemical Physics*, *19*(20), pp.12959-12969.

23. Rissanou, A.N. and Harmandaris, V., 2013. A Molecular Dynamics Study of Polymer/G raphene Nanocomposites. *Macromolecular Symposia*, *331*(1), pp.43-49.

24. Jin, Y., Duan, F. and Mu, X., 2016. Functionalization enhancement on interfacial shear strength between graphene and polyethylene. *Applied Surface Science*, *387*, pp.1100-1109.

25. Liu, F., Liu, X., Hu, N., Ning, H., Atobe, S., Yan, C., et. al., 2017. Investigation of thermal energy transport interface of hybrid graphene-carbon nanotube/polyethylene nanocomposites. *Scientific reports*, *7*(1), p.14700.

26. Parashar, A. and Mertiny, P., 2013. Multiscale model to study of fracture toughening in graphene/polymer nanocomposite. *International Journal of Fracture*, *179*(1-2), pp.221-228.

27. Li, M., Zhou, H., Zhang, Y., Liao, Y. and Zhou, H., 2017. The effect of defects on the interfacial mechanical properties of graphene/epoxy composites. *RSC Advances*, *7*(73), pp.46101-46108.

28. Li, M., Zhou, H., Zhang, Y., Liao, Y. and Zhou, H., 2018. Effect of defects on thermal conductivity of graphene/epoxy nanocomposites. *Carbon*, *130*, pp.295-303.

29. Ma, J., Meng, Q., Michelmore, A., Kawashima, N., Izzuddin, Z., Bengtsson, C. and Kuan, H.C., 2013. Covalently bonded interfaces for polymer/graphene composites. *Journal of Materials Chemistry A*, *1*(13), pp.4255-4264.

30. Lv, C., Xue, Q., Xia, D. and Ma, M., 2012. Effect of chemisorption structure on the interfacial bonding characteristics of graphene–polymer composites. *Applied Surface Science*, *258*(6), pp.2077-2082.

31. Ding, N., Chen, X., Wu, C.M.L. and Lu, X., 2012. Computational investigation on the effect of graphene oxide sheets as nanofillers in poly (vinyl alcohol)/graphene oxide composites. *The Journal of Physical Chemistry C*, *116*(42), pp.22532-22538.

32. Ramanathan, T., Abdala, A.A., Stankovich, S., Dikin, D.A., Herrera-Alonso, M., Piner, R.D., et. al., 2008. Functionalized graphene sheets for polymer nanocomposites. *Nature nanotechnology*, *3*(6), p.327.

33. Liu, F., Hu, N., Zhang, J., Atobe, S., Weng, S., Ning, H., et. al., 2016. The interfacial mechanical properties of functionalized graphene–polymer nanocomposites. *RSC Advances*, *6*(71), pp.66658-66664.

34. Banhart, F., Kotakoski, J. and Krasheninnikov, A.V., 2010. Structural defects in graphene. *ACS nano*, *5*(1), pp.26-41.

35. Rajasekaran, G., Narayanan, P. and Parashar, A., 2016. Effect of point and line defects on mechanical and thermal properties of graphene: a review. *Critical Reviews in Solid State and Materials Sciences*, *41*(1), pp.47-71.

36. Simonis, P., Goffaux, C., Thiry, P.A., Biro, L.P., Lambin, P. and Meunier, V., 2002. STM study of a grain boundary in graphite. *Surface science*, *511*(1-3), pp.319-322.

37. Kim, K., Lee, Z., Regan, W., Kisielowski, C., Crommie, M.F. and Zettl, A., 2011. Grain boundary mapping in polycrystalline graphene. *ACS nano*, *5*(3), pp.2142-2146.

38. Xu, N., Guo, J.G. and Cui, Z., 2016. The influence of tilt grain boundaries on the mechanical properties of bicrystalline graphene nanoribbons. *Physica E: Low-dimensional Systems and Nanostructures*, *84*, pp.168-174.

39. Yang, B., Wang, S., Guo, Y., Yuan, J., Si, Y., Zhang, S. and Chen, H., 2014. Strength and failure behavior of a graphene sheet containing bi-grain-boundaries. *RSC Advances*, *4*(97), pp.54677-54683.

40. Grantab, R., Shenoy, V.B. and Ruoff, R.S., 2010. Anomalous strength characteristics of tilt grain boundaries in graphene. *Science*, *330*(6006), pp.946-948.

41. Verma, A., Parashar, A. and Packirisamy, M., 2018. Tailoring the failure morphology of 2D bicrystalline graphene oxide. *Journal of Applied Physics*, *124*(1), p.015102.

42. Verma, A. and Parashar, A., 2018. Reactive force field based atomistic simulations to study fracture toughness of bicrystalline graphene functionalised with oxide groups. *Diamond and Related Materials*, *88*, pp.193-203.

43. Chenoweth, K., Van Duin, A.C. and Goddard, W.A., 2008. ReaxFF reactive force field for molecular dynamics simulations of hydrocarbon oxidation. *The Journal of Physical Chemistry A*, *112*(5), pp.1040-1053.

44. Girifalco, L.A., Hodak, M. and Lee, R.S., 2000. Carbon nanotubes, buckyballs, ropes, and a universal graphitic potential. *Physical Review B*, *62*(19), p.13104.

45. Luo, T. and Lloyd, J.R., 2012. Enhancement of thermal energy transport across graphene/graphite and polymer interfaces: a molecular dynamics study. *Advanced Functional Materials*, *22*(12), pp.2495-2502.

46. Wang, Y., Zhan, H.F., Xiang, Y., Yang, C., Wang, C.M. and Zhang, Y.Y., 2015. Effect of covalent functionalization on thermal transport across graphene–polymer interfaces. *The Journal of Physical Chemistry C*, *119*(22), pp.12731-12738.

47. Senftle, T.P., Hong, S., Islam, M.M., Kylasa, S.B., Zheng, Y., Shin, Y.K., et. al., 2016. The ReaxFF reactive force-field: development, applications and future directions. *NPJ Computational Materials*, *2*, p.15011.

48. Verma, A. and Parashar, A., 2018. Molecular dynamics based simulations to study failure morphology of hydroxyl and epoxide functionalised graphene. *Computational Materials Science*, *143*, pp.15-26.

49. Verma, A. and Parashar, A., 2018. Molecular dynamics based simulations to study the fracture strength of monolayer graphene oxide. *Nanotechnology*, *29*(11), p.115706.

50. Plimpton, S., 1995. Fast parallel algorithms for short-range molecular dynamics. *Journal of computational physics*, *117*(1), pp.1-19.

51. Kumar, R., Mertiny, P. and Parashar, A., 2016. Effects of different hydrogenation regimes on mechanical properties of h-BN: a reactive force field study. *The Journal of Physical Chemistry C*, *120*(38), pp.21932-21938.

52. Singla, V., Verma, A. and Parashar, A., 2018. A molecular dynamics based study to estimate the point defects formation energies in graphene containing STW defects. *Materials Research Express*, *6*(1), p.015606.

53. Stukowski, A., 2009. Visualization and analysis of atomistic simulation data with OVITO–the Open Visualization Tool. *Modelling and Simulation in Materials Science and Engineering*, *18*(1), p.015012.

54. Verma, A. and Parashar, A., 2017. The effect of STW defects on the mechanical properties and fracture toughness of pristine and hydrogenated graphene. *Physical Chemistry Chemical Physics*, 19, pp.16023-16037.

55. Tsai, D.H., 1979. The virial theorem and stress calculation in molecular dynamics. *The Journal of Chemical Physics*, *70*(3), pp.1375-1382.

56. Meng, F., Chen, C. and Song, J., 2017. Lattice trapping and crack decohesion in graphene. *Carbon*, *116*, pp.33-39.

57. Verma, A. and Parashar, A., 2018. Structural and chemical insights into thermal transport for strained functionalised graphene: a molecular dynamics study. *Materials Research Express*, *5*(11), p.115605.

58. Liao, L., Huang, C. and Meng, C., 2018. Study on mechanical properties of polyethylene with chain branching in atomic scale by molecular dynamics simulation. *Molecular Simulation*, pp.1-9.

59. Lu, C.T., Weerasinghe, A., Maroudas, D. and Ramasubramaniam, A., 2016. A comparison of the elastic properties of graphene-and fullerene-reinforced polymer composites: the role of filler morphology and size. *Scientific reports*, *6*, p.31735.

Highlights

- ✓ So far, none of the research articles have been reported on the effect of grain boundaries on reinforcing capabilities of graphene for polymer based nanocomposites.
- ✓ Significant improvement in the tensile strength, interfacial shear and normal cohesive strength of PE nanocomposite was reported with bi-crystalline graphene as compared to pristine graphene nanosheet.
- ✓ The simulations performed with help of ReaxFF and Lennard-Jones potential, predicted that higher mis-orientation angle grain boundary resulted in more number of adhesion points and better non-bonding interaction at the interface of reinforcement and matrix.
- ✓ This investigation would be helpful in exploring the properties of bi-crystalline graphene nanosheets playing a conclusive role in tailoring the mechanical properties of nanocomposites and provides useful design guidelines for their utilization.

Graphical abstract